Thesis for the degree of Doctor of Philosophy

Phase Retrieval Methods for Electromagnetic Source Modeling

Markus Johansson

Department of Signals and Systems
Biomedical Electromagnetics Group
Chalmers University of Technology
Göteborg, Sweden, 2011

Supervisor: Professor Mikael Persson, Chalmers

Phase Retrieval Methods for Electromagnetic Source Modeling
Markus Johansson
ISBN 978-91-7385-485-6

Doktorsavhandlingar vid Chalmers tekniska högskola
Ny serie Nr 3166
ISSN 0346-718X

Department of Signals and Systems
Biomedical Electromagnetics Group
Chalmers University of Technology
SE–412 96 Göteborg
Sweden
Telephone +46–(0)31–772 10 00

Prepared with LaTeX
Printed by Chalmers Reproservice
Göteborg, Sweden, 2011

PHASE RETRIEVAL METHODS FOR ELECTROMAGNETIC SOURCE MODELING

Markus Johansson
Department of Signals and Systems
Chalmers University of Technology

Abstract

Modeling of the field distributions from electromagnetic sources is of interest for various applications including electromagnetic compatibility investigations, near-field to far-field transformations, antenna diagnostics and electromagnetic dosimetry. In order to determine whether exposure safety guidelines, such as the EU directive 2004/40/EC, are complied with, source modeling methods are important.

Two methods for determining the total field, including phase information, when only field amplitudes have been measured on a set of planes in front of an electromagnetic source have been developed. The first method, the adjoint field method, is a gradient based optimization algorithm based on the adjoint fields. The second method, the phase angle gradient method, employs an optimization algorithm based on the phase angle gradients of a functional.

The two methods have been tested for numerical test cases with both high and low frequencies and the phase angle gradient method was found to perform best. Moreover, it gave results that are in excellent agreement with the correct phase. The phase angle gradient method was also tested for measured magnetic flux density with low frequency from a transformer and for electric field with high frequency from a mobile phone. For the cases with measured field the obtained phase angles on the measurement plane closest to the source gave calculated field on other measurement planes that agrees well with measured field.

Keywords: dosimetry, optimization, SAR, source modeling, phase retrieval

Publications

The thesis is based on the following papers.

Paper **A**

M. Johansson, L. E. Nord, R. Kopecký, A. Fhager and M. Persson, "Computational methods for modeling of complex sources", *COMPEL: The International Journal for Computation and Mathematics in Electrical and Electronic Engineering*, vol. 27, no. 1, pp. 133-143, 2008.

Paper **B**

M. Johansson, H.-S. Lui and M. Persson, "Performance evaluation of phase-angle gradient method for phase retrieval based on low-frequency amplitude-only near-field data", *Progress In Electromagnetics Research B*, vol. 25, pp. 113-130, 2010.

Paper **C**

M. Johansson, H.-S. Lui, J.-C. Bolomey and M. Persson, "Source modeling using phaseless low-frequency near-field measurements", *Submitted to IEEE Transactions on Electromagnetic Compatibility*, 2010.

Paper **D**

M. Johansson and M. Persson, "Phase-retrieval from phaseless measured E-field data", *2008 URSI General Assembly*, Chicago, USA, August 7-16, 2008.

Paper **E**

M. Johansson, A. Fhager, H.-S. Lui and M. Persson, "Comparision between two phase-retrieval methods", *Submitted to PIER/JEMWA*, 2011.

Conference Contributions

The conference contributions which are not included in the thesis are listed below:

1. L. E. Nord, M. Johansson, A. Fhager, R. Kopecký and M. Persson, "Near Field Modeling of Complex Sources", *Bioelectromagnetics Society (BEMS) 28th Annual Meeting*, Cancun, Mexico, June 11-15, 2006.

2. M. Johansson, L. E. Nord, A. Fhager, R. Kopecký and M. Persson, "Modeling of complex sources for dosimetry applications", *Medicinteknikdagarna 2006*, Uppsala, Sweden, 2006.

3. M. Johansson, A. Fhager and M. Persson, "Optimization Algorithms for Modeling of Electromagnetic Sources", *ACES 2007*, Verona, Italy, March 19-23, 2007.

4. M. Johansson, A. Fhager and M. Persson, "Near Field Modeling with Optimization Algorithms", *The Bioelectromagnetics Society 29th Annual Meeting*, Kanazawa, Japan, Jun 10-15, 2007.

5. M. Johansson, J. Alonso Macías, Y. Hamnerius and M. Persson, "Modeling of Electromagnetic Sources with Huygens Principle", *Abstracts PIERS 2007, Progress In Electromagnetics Research Symposium*, Prague, Czech Republic, 2007.

6. M. Johansson, A. Fhager and M. Persson, "Near Field Modeling with Huygens Principle", *EMB 07*, Lund, Sweden, Oct 18-19, 2007.

7. M. Johansson and M. Persson, "Phase-Retrieval from Amplitude-Only Field Measurements", *Proceedings of RVK08/MMWP08*, Växjö, Sweden, June 9-13, 2008.

8. M. Johansson and M. Persson, "Modeling of electromagnetic sources for numerical dosimetry", *Medicinteknikdagarna 2008*, Göteborg, Sweden, Oct 14-15, 2008.

9. M. Johansson, Y. Hamnerius and M. Persson, "Work exposure to electromagnetic fields", *Electromagnetics in Advanced Applications, 2009. ICEAA '09. International Conference on* , pp. 548–551, 2009.

10. M. Johansson, Y. Hamnerius and M. Persson, "Numerical calculations of fields in humans exposed to electromagnetic sources", *Medicinteknikdagarna 2009*, Västerås, Sweden, Sept 28-29, 2009.

11. M. Johansson, H.-S. Lui and M. Persson, "Performance Evaluation of Phase Retrieval Method based on Amplitude-Only Near-Field Data", *Proceedings of the Asia Pacific Microwave Conference*, 2009.

Acknowledgements

First of all, I would like to thank my supervisor Prof. Mikael Persson for giving me the opportunity to become a Ph.D. student in his group and for all his help and support. I am also grateful for all help from my co-supervisor Hoi-Shun Lui. Furthermore I would like to thank The Swedish Labour Market Insurance AFA for their financial support to this project.

I also want to thank all the other kind and nice members of our research group, during my time at Chalmers. Some names in alphabetical order are: Adisak Romputtal, Andreas Fhager, Ansar Mahmood, Artur Chodorowski, Fangyuan Jiang, Hana Dobšíček Trefná, Prof. Lennart Lundgren, Lovisa Nord, Mahmood Qaiser, Mai Lu, Oskar Talcoth, Paolo Togni, Parham Hashemzadeh, Reza Shiee, Rudolf Kopecký, Shantanu Padhi, Tonny Rubaek, Xuezhi Zeng and Yazdan Shirvany. All the previous and present group members have made very important contributions to make our research group such a nice group to work in.

A special thank goes to Hana, Xuezhi and Andreas. Our thesis writing/code writing competitions have been very nice. Although I did not win any of them, I am very pleased that when I send this thesis for printing, I will come on bronze place for the second time in a row. Moreover, I am almost certain that I will win next competition.

I am also grateful to Prof. Yngve Hamnerius and Ralf Berndtsson from our neighbouring group, for all help and support.

I would also like to thank Per Nyqvist and Petter Falkman for their help with the robot measurements. Furthermore, I want to thank Jonas Fridén and Martin Siegbahn at Ericsson in Göteborg and in Stockholm, for providing me with measured electric field.

In addition, I would like to thank Prof. Jean-Charles Bolomey for his important contributions to paper **C** in this thesis.

I am also grateful to Prof. Shoogo Ueno and his wife Haruko for their incredible generosity always and especially during my visit in their home in Japan.

Furthermore, I want to extend my thanks to everyone else that I have had contact with, at our department as well as at the rest of Chalmers.

Finally, I also want to thank my parents.

Contents

Chapter 1

Introduction

Electromagnetic fields are used for transferring information in wireless communication applications such as mobile communication, radio and television. Many other sources, for example welding machines and power lines, also give rise to electromagnetic fields. It is important to be able to model the field distribution from the electromagnetic sources for different reasons. Firstly it is important to model the distribution of the fields to make sure that various electromagnetic devices work as intended. Secondly it is essential to know the field that one device give rise to in order to make sure that other electromagnetic equipment is not disturbed by the device. Moreover it is crucial to investigate whether there are risks for adverse health effects associated with the fields and if so try to avoid these risks.

One way to model an electromagnetic source is to first measure the field values on a surface between the source and the area of interest. The measured field components can then be used in an electromagnetic solver to calculate the field distribution in the area of interest. Measurements of both amplitude and phase of the field generally require more efforts and are more expensive than amplitude-only measurements. Therefore methods that can be used to retrieve the phase from measurements of the field amplitudes on a set of measurement planes in front of the source are of large interest. An important advantage with this kind of source modeling method is that it can be used for different electromagnetic sources without detailed knowledge of the sources. In order to obtain the field inside humans exposed to electromagnetic sources, a model of the dielectric properties of a human can be inserted in the computational domain of the electromagnetic solver.

It is well known that electromagnetic fields could be harmful to humans when the intensity is high. One well known example of that electromagnetic fields can be used to obtain high temperatures in biological materials, is heating of food in microwave ovens. It is however not so easy to determine how large the field intensity and exposure time need to be, to cause adverse health effects. To investigate the health effects of exposure to electromagnetic fields, epidemiologic research has been performed [1–7]. Exposure

safety guidelines, which are intended to provide protection against known adverse health effects, have also been formulated [8]. In order to determine whether the exposure safety guidelines are complied with in different exposure situations, it is important to be able to calculate the electromagnetic fields inside humans.

1.1 Exposure safety guidelines

The International Commission on Non-Ionizing Radiation Protection (ICNIRP) has provided guidelines in [8], which are intended to provide protection against known adverse health effects. Basic restrictions are provided, on current density, for frequencies between 1 Hz and 10 MHz, to prevent effects on nervous system functions and on specific energy absorption rate (SAR), for frequencies between 100 kHz and 10 GHz, to prevent unwanted heating effects. Restrictions are provided on both SAR and current density in the 100 kHz-10 MHz range. There are SAR restrictions both for whole-body average SAR and localized SAR.

For comparison with measured values of physical quantities, ICNIRP also provides reference levels. The field in front of an electromagnetic source can be measured and compared with the reference levels rather easily, whereas it is more complicated to find out how large current density or SAR the source can give rise to in a human. Compliance with all the reference levels is intended to ensure compliance with basic restrictions. If on the other hand measured values exceed the reference levels, it is not certain that the basic restrictions have been exceeded.

Results presented in [9] suggest however that in some numerical test cases with children exposed to fields with frequencies above 1 GHz, the ICNIRP reference level does not provide a conservative estimate of the whole-body-averaged SAR restriction. Thus it is important to be able to calculate the fields in humans, to make it possible to check whether the basic restrictions have been exceeded or not, both in situations with measured field values above and below the reference levels.

The ICNIRP exposure restrictions are more stringent for the general public, than for the occupationally exposed population. The argument for this is that members of the public may not even be aware of their exposure to electromagnetic fields, whereas people who are exposed to electromagnetic fields in their work environment hopefully are both aware of potential risks and trained to take precautions when appropriate.

The EU directive 2004/40/EC contains minimum requirements to protect workers exposed to electromagnetic fields and is based on the guidelines of ICNIRP, see [10]. The directive was due to enter into force in April 2008, but the European Commission has proposed to postpone the deadline for introducing legislation on workers' exposure to electromagnetic fields until 30 April 2012, which will give time for amendment to the directive in order

to take account of recent research findings on the possible impact of the exposure limits on MRI [11]. Furthermore it is intended to review the situation for all sectors where personnel are exposed to electromagnetic fields and the proposed postponement will allow time to take into account new recommendations from relevant international bodies [11]. The postponement that the European Commission proposed was adopted, see the EU directive 2008/46/EC [12].

Recommendations to protect humans exposed to electromagnetic fields, against harmful effects, can also be found in an IEEE standard [13]. The OET Bulletin 65 [14] contains information that can be used in determination of whether proposed or existing transmitting facilities, operations or devices comply with limits for human exposure to radio frequency (RF) fields adopted by the Federal Communications Commission (FCC).

1.2 Electromagnetic fields and health

Studies have been performed to investigate the health effects of exposure to electromagnetic fields. The effects of extremely low frequency (ELF) fields are summarized by WHO [4] and the effects of radio frequency fields have been reviewed by ICNIRP [5].

The ELF range include frequencies from 3 Hz to 300 Hz. Research results indicate that ELF might increase the risk for childhood leukemia [2]. An evaluation of evidence on the carcinogenicity of ELF fields, was performed by the International Agency for Research on Cancer (IARC) [3]. IARC judged ELF magnetic fields to be "possible carcinogenic to humans".

The review article [1] summarizes the epidemiologic studies on the effects of radio frequency fields (RFs) and human health. Although radio frequency fields do not have sufficient energy to destabilize electron configurations within DNA molecules [1], there has been concern about possible carcinogenic effects associated with the fields. Possible mechanisms for such effects is a topic that is still open for discussion.

Studies have been performed for various cancer types. The risks of glioma and meningioma for mobile phone users have been studied in a joint study performed in 13 countries; the Interphone study [6]. The study showed no increased risks for mobile phone users, on the contrary a significant protective effect was seen for mobile phone use. These results have been questioned and the Interphone researchers write that it is possibly due to participation bias or other methodological limitations [6]. The risk of acoustic neuroma in relation to mobile phone use have also been studied in the Interphone project, the results from the whole study have not yet been published, data from five north European countries were released in 2005 [7]. The study suggests that in the first decade after starting mobile phone use there is no substantial risk of acoustic neuroma, but an increase in risk after longer time could not be ruled out.

1.3 Interaction between fields and the body

In order to understand how a human is affected by exposure to electromagnetic fields, it is important to understand the interaction between electromagnetic fields and the human body. The interaction of electromagnetic fields with biological systems changes its character with the frequency.

Ionizing radiation like x-rays can break chemical bonds, forming ions that can damage biological systems [2]. In the rest of this thesis however ionizing radiation will not be considered. Instead non-ionizing radiation will be the focus. Non-ionizing radiation [8] includes all fields of the electromagnetic spectrum that do not normally have sufficient energy to produce ionization in matter and is characterized by energy per photon less than about 12 eV or frequencies lower than $3 \cdot 10^{15}$ Hz [8].

For situations with exposure to fields with low frequencies in the range from a few Hz to 1 kHz effects on nervous system functions is a limiting effect. In that range the thresholds for acute changes in central nervous system excitability and other acute effects are exceeded, for levels of induced current density larger than 100 mA m^{-2} [8]. Using a safety factor of 10, the ICNIRP basic restriction on current density for occupational exposure in the frequency range 4 Hz to 1 kHz was set to 10 mA m^{-2}.

For high frequencies the heating effect of the field becomes important. The heating effect is closely linked to the SAR value, which is absorbed energy in body tissues per unit time and unit mass. According to [8], animal data indicate a threshold for behavioral responses for a whole-body SAR of between 1 and 4 W kg^{-1} and experimental evidence indicates that the exposure of resting humans for approximately 30 min to fields producing a whole-body SAR in that range results in a body temperature increase of < 1 °C. More intense fields that produce larger SAR values can cause overwhelming of the thermoregulatory capacity of the body and harmful levels of tissue heating [8]. The ICNIRP basic restriction on whole-body average SAR for occupational exposure in the frequency range 10 MHz to 10 GHz, 0.4 W kg^{-1}, is obtained by using a safety factor of 10.

1.4 Calculation of current density and SAR

The RMS (root mean square) value of the current density J_{rms} and the SAR are related to the RMS value of the electric field E_{rms} through the relations

$$J_{rms} = \sigma E_{rms} \tag{1.1}$$

$$SAR = \frac{\sigma E_{rms}^2}{\rho}, \tag{1.2}$$

where σ is the conductivity and ρ the mass density. Thus, if the fields inside a human are known, SAR and current density can easily be obtained.

In order to determine whether exposure safety guidelines such as basic restrictions in the IEEE standard or basic restrictions provided by ICNIRP are complied with, it is therefore important to be able to calculate the electromagnetic fields inside humans exposed to fields from electromagnetic sources. To calculate the fields inside a human, different types of electromagnetic solvers can be used together with a model of the dielectric properties of the human. The finite-difference time-domain (FDTD) method [15] is one numerical method, that can be used to solve Maxwell's equations and obtain the fields. The FDTD method is very suitable for numerical dosimetry, in situations with exposure to high frequency fields. For low frequency dosimetry one suitable method is the impedance method described in [16]. Another method that can be used in numerical dosimetry is the finite-element method. In [17] is for example a hybrid finite-element method (FEM)/method of moments (MoM) technique employed for SAR calculations in a human phantom in the near field of a base-station antenna.

1.5 Electromagnetic sources

Both at work places and elsewhere we are surrounded by electromagnetic sources. Some examples are mobile phones, base stations, other devices for wireless communication, plastic welding machines, devices for glue drying, anti-theft devices, point welding machines, arc welding machines and power lines. The sources give rise to fields with very different frequencies. Some examples of frequencies used by mobile phones are 900 MHz and 1800 MHz. Welding machines, on the other hand, can give fields with various frequencies, for example 50 Hz.

When a suitable numerical method is used to calculate the fields in a human exposed to an electromagnetic source, the source needs to be modeled. In view of the many kinds of electromagnetic sources that are present in the world around us and since many electromagnetic devices also come in new models year after year, it would be very nice with a source modeling method that could be used for many of the different sources without requiring much changes in the setup between the modeling of different sources.

There are different ways of doing source modeling. If for example the FDTD method is used, one possibility is to insert models of both the source and the dielectric properties of a human in the computational domain and do the calculations. This requires however detailed knowledge of the source and, if the source is complex, it can be both difficult and time consuming to make such a model of the electromagnetic source.

Another possibility is to utilize the field equivalence principle [18] and use measured field values on a planar surface positioned between the source and the area for the calculation of the fields. If the total electric field, both amplitude and phase, is known on the plane and the plane is large enough, the known field values can be inserted in the FDTD calculation and the

fields in the area of interest can be obtained, see figure 1.1. This method

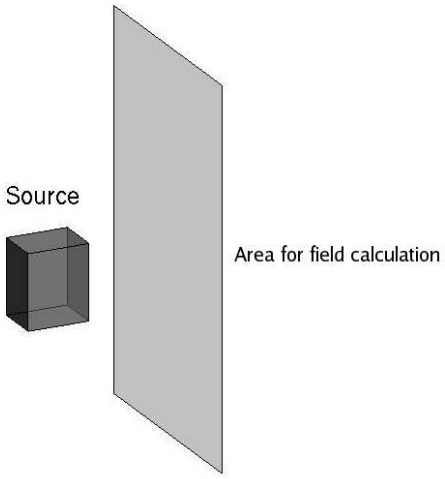

Figure 1.1: Field values on a plane in front of the source can be used to calculate the fields in the area of interest.

has the important advantage that it can be used for many different sources without detailed knowledge of the sources.

For field measurements, for example, at work places, usually only the RMS values of the fields are measured. Measurement instruments from Narda [19] and the BMM-3 from EnviroMentor [20] are examples of instruments that are used for field measurements where RMS values, but not the phase difference between the field values in different measurement points, are measured. To obtain the total field, including phase information, when only field amplitudes have been measured on a set of planes in front of an electromagnetic source, two different methods have been developed in this thesis. One method is a gradient based optimization algorithm, based on the adjoint fields. A second method employs an optimization algorithm based on the phase angle gradients of a functional. The two methods are presented and tested for various test cases in the papers **A** – **E**. Other phase-retrieval methods can also be found in the scientific literature, see for example [21–33]. The different methods are discussed further in chapter 2.

In situations with exposure to monochromatic fields, the application of the phase retrieval methods for source modeling is straight forward. Our phase retrieval methods were originally developed for monochromatic fields and not for fields with arbitrary time dependence. The methods may, however, also be used when the field from the source can be written as a sum of different frequency components, if each component can be handled separately.

Chapter 2

Source modeling using measured field values

Measured fields on a Huygens' surface enclosing an electromagnetic source, can be used to calculate the fields outside the surface [18]. The Huygens' surface can be approximated by a sufficiently large planar surface between the source and the area for the calculation of the fields. The fields beyond the surface can be obtained numerically, if the total electric or magnetic field, that is both amplitude and phase of the field, on it is known.

Source modeling has been studied by a large number of authors. Methods that utilize the measured total field in the vicinity of a source to determine an equivalent magnetic current source, have, for example, been presented by Taaghol et al. [34], and more recently by Las-Heras et al. [35]. An equivalent current approach was compared with a modal expansion method in [36]. Antenna diagnostics from near-field measurements was discussed in [37] and [38]. Methods to represent antennas with equivalent radiation sources consisting of dipoles were presented in [39] and [40]. Reconstruction of equivalent currents for a reflector antenna covered by a radome was discussed in [41]. A formulation of the source reconstruction problem on arbitrary three-dimensional surfaces based on integral equations, that is suitable for diagnostic applications even if fields close to the actual source are required, was presented in [42] and [43].

In field measurements at for example work places is however usually only the RMS values of the fields measured. Therefore we have developed two methods, that recreates the phase information and thereby find the desired total field, by using the measured field amplitudes on a set of planes in front of the source, see figure 2.1.

The first method, the adjoint field method is a gradient based optimization algorithm, based on the adjoint fields. The second method, the phase angle gradient method, employs an optimization algorithm based on the phase angle gradients of a functional. The methods extend previously made constant phase approximations in [44].

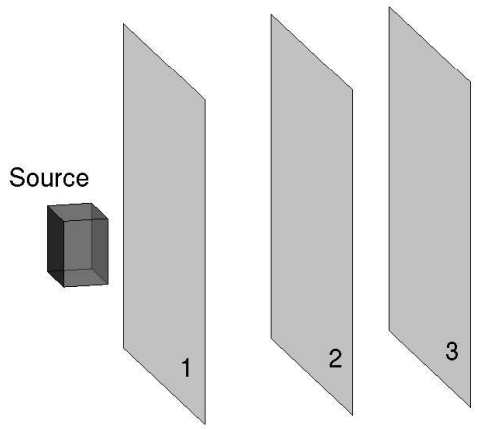

Figure 2.1: Source in front of planes where field amplitudes can be measured.

In this chapter other phase retrieval methods and these two methods, which are presented and tested with various test cases in the papers **A** – **E**, are described. The last section of the chapter deals with phase retrieval for field with low frequency.

2.1 Phase retrieval in the scientific literature

Various authors have used different methods to try to recreate the phase angles from phase-less field data, see for example [21–33]. Some of the methods, see e.g. [21–25], are gradient based and try to minimize a functional, whereas other methods, see e.g. [26–29], try to recreate the phase angles in an iterative fashion, by propagating field estimates back and forth between different surfaces. Hybrid algorithms, that combine more than one method, have also been presented, one of them in [30] and another one in [31].

Determination of radiation pattern, from phaseless near field data collected over limited domains on planar surfaces, by minimization of a functional, is discussed in [21]. A formulation of the problem of determining radiation pattern, from phaseless square amplitude measurements over two planes, as a quadratic inverse problem, is described in [22]. The radiated field in the near zone is searched for using gradient based functional minimization. Strategies to avoid getting trapped in local minima is discussed both in [22] and in [25], where also another method, that uses measurements with two different probes moved over a single surface, is discussed. A method used in [23] and [24], use an expansion of an equivalent magnetic

current distribution on a plane in front of the source and expansion coefficients, that minimize a cost function, are searched for with a gradient based algorithm. In this method the measurement points can be on planes, but can also be on any other arbitrary surface. A procedure that uses measured amplitude distributions on spherical surfaces and searches for coefficients for a spherical wave expansion, that minimize a cost function, is presented in [33].

Phase retrieval in optics by a method that propagate field estimates back and forth between different planes, using Fast Fourier Transform (FFT), was put forward by Gerchberg and Saxton [26]. Between consecutive propagations in the algorithm, the field amplitudes are reset to the measured fields. In [32] the Gerchberg-Saxton algorithm and related algorithms for phase retrieval and also gradient search methods are discussed. After the early work with phase retrieval methods in optics, other authors have used similar methods for phase retrieval in other applications [27–29].

An iterative Fourier procedure for phase retrieval in a forward-backward fashion, used for constructing of the far-field pattern and diagnostic characteristics of an antenna under test, has been presented in [28]. In a hybrid method described in [30], a slightly modified version of the iterative Fourier procedure used in [28] is combined with a method called the Differential Evolutionary Algorithm, which is used to search for a suitable initial guess. A method similar to the iterative procedure in [28], but used for the electric field in a phantom with lossy liquid, can be found in [29]. To improve the convergence of the phase retrieval method presented in [29], a three-step algorithm that also utilizes a gradient search method, has been proposed in [31]. A cylindrical phase retrieval algorithm, that propagate field estimates back and forth and uses field intensity measurements made on two cylindrical surfaces instead of planes, have been described in [27].

In the rest of this section three of the different phase retrieval algorithms are described in more detail. To illustrate the principles for the different types of phase retrieval algorithms, three different kinds of methods have been chosen. The first is gradient based like the phase angle gradient method, the second searches for the phase in an iterative forward-backward fashion and the third is a three-step algorithm in which different methods are used in different steps.

2.1.1 Gradient based phase retrieval

A method that utilizes an equivalent magnetic current distribution, have been presented in [23] and [24]. Their method uses an expansion of the magnetic current distribution. In their method, the Cartesian components of the current distribution on the z=0-plane, M_y and M_x, are, using M subdomain-type basis functions, $f_m(x', y')$, weighted by unknown complex

coefficients $C_{x,m}$, $C_{y,m}$, approximated as

$$M_y(x', y') \cong \sum_{m=1}^{M} C_{y,m} \cdot f_m(x', y') \tag{2.1}$$

$$M_x(x', y') \cong \sum_{m=1}^{M} C_{x,m} \cdot f_m(x', y'). \tag{2.2}$$

and a conjugate gradient algorithm with analytical derivatives is used to search for expansion coefficients, that minimize the cost function

$$F = \sum_{n=1}^{N} \left[\left(E_{x,n}^{meas}\right) \cdot \left(E_{x,n}^{meas}\right)^* - \left(E_{x,n}\right) \cdot \left(E_{x,n}\right)^* \right]^2, \tag{2.3}$$

where $E_{x,n}^{meas}$ is measured and $E_{x,n}$ is calculated x-component of the electric field in measurement point n. The measurement points for the method can for example be on one or more planes, but they can also be on any other arbitrary surface. Two independent minimizations, each one using one component of the equivalent source and either the x-component or the y-component of the electric field, is performed in the method. In [23] and [24] results for various test cases for the method were presented and it was for example reported that far-field results obtained for an aperture antenna, using amplitude-only data over two planes, agree with results obtained using both amplitude and phase information.

2.1.2 Phase retrieval in a forward-backward fashion

Phase retrieval in a forward-backward fashion is discussed in this section. An example of an iterative process for recovering of the phase, using amplitudes of the electric field components measured in a phantom with lossy liquid, is described in [29]. The field amplitudes are measured in two planes in the phantom. The used phase retrieval algorithm is applied to one Cartesian component of the field at a time and works as follows.

The phase angles on the plane closest to the source are set to some initial values and the complex field they give together with the measured amplitudes, is propagated using plane wave spectrum techniques to the second plane. Then the field amplitudes are reset to the measured ones and the field is propagated back to the previous plane. The reseting of the amplitudes to the measured values followed by propagation to previous plane is repeated a number of times, so that the field is propagated back and forth between the two planes. This is done until the accuracy is good enough or the number of iterations is large enough.

2.1.3 Combination of different methods

The method described in 2.1.2 suffers, according to [29], from a stagnation problem. To improve the convergence of the phase retrieval, a three-step

algorithm has been proposed in [31]. The algorithm consists of the following steps:

1. A number of phase distributions ϕ_1^n on plane 1, the plane closest to the source, are tested. Some of the phase distributions, that together with the measured amplitudes on plane 1 give the best resulting field amplitudes when propagated to the second plane, are kept for further use in the next step.

2. Each of the kept ϕ_1^n are used as the initial values of the phase angles on plane 1. For each of the initial phase distributions, the field is propagated back and forth between the two planes according to the same principle as for the method in [29], that is described in 2.1.2.

3. A gradient search method is applied to the best of the resulting phase distributions in step 2.

It was found in [31] that the addition of more steps to the previous algorithm described in 2.1.2 improved both accuracy and robustness.

2.2 Developed phase retrieval methods

In this section the two phase retrieval methods we developed, the adjoint field method and the phase angle gradient method, are described.

2.2.1 The adjoint field method

The adjoint field method involves finding equivalent dielectric properties between two parallel planes, e.g. the planes 1 and 2 in figure 2.1. If the measured electric field amplitudes on plane 1 are used as source with the field components set to be in phase, these properties should yield the correct total field, phase as well as amplitude, on the planes 2 and 3. The FDTD method is used for the calculations, and a gradient based optimization algorithm is used to find the equivalent dielectric properties.

Versions of this type of optimization algorithm is also used in microwave tomography and can be found in [45–49]. In the tomography application described in [47–49], the dielectric properties ϵ and σ in an area, are searched for. As illustrated in figure 2.2, the area where the dielectric properties are searched for is surrounded by transmitting/receiving antennas represented by black dots. One antenna at the time is used as transmitter, while the others are used as receivers, that measure the field. This is done repeatedly until each antenna has been used as a transmitter. A gradient based optimization algorithm is used to try to find dielectric properties, that in numerical calculations give field values as close to the field values measured by the receivers as possible.

For the source modeling application considered here we search for the equivalent dielectric properties, that gives the correct total field on the

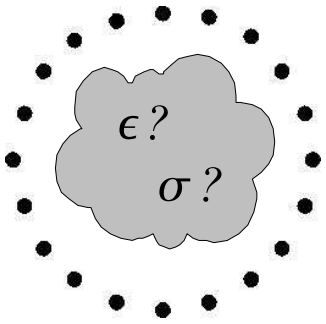

Figure 2.2: Area where the dielectric properties are searched for in the tomography application, surrounded by transmitting/receiving antennas, represented by black dots.

planes 2 and 3 in figure 2.1. This is somewhat different than the tomography application. The measurement points on the planes 2 and 3 in figure 2.1 correspond to the points where the receiving antennas are located in the tomography application. In the tomography application each antenna is used as a transmitting source. Here the measured electric field amplitudes on plane 1, with the field components set to be in phase, is used instead as only one source.

In the original [47–49] optimization algorithm the functional to be minimized is

$$F(\epsilon,\sigma) = \int_0^T \sum_{m=1}^{M}\sum_{n=1}^{N} \left(|\bar{E}_m(\epsilon,\sigma,\bar{R}_n,t) - \bar{E}_m^{meas}(\bar{R}_n,t)|^2\right) dt, \tag{2.4}$$

where $\bar{E}_m(\epsilon,\sigma,\bar{R}_n,t)$ is the calculated field and $\bar{E}_m^{meas}(\bar{R}_n,t)$ the measured field on planes 2 and 3. M is the number of sources and N is the number of measurement points on planes 2 and 3. The minimization is done with a conjugate-gradient algorithm. The gradients can be written as

$$G_\epsilon(\bar{x}) = 2\sum_{m=1}^{M}\int_0^T \tilde{\bar{E}}_m(\epsilon,\sigma,\bar{x},t)\cdot\partial_t\bar{E}_m(\epsilon,\sigma,\bar{x},t)dt \tag{2.5}$$

$$G_{\sigma/\langle\sigma\rangle}(\bar{x}) = 2\langle\sigma\rangle\sum_{m=1}^{M}\int_0^T \tilde{\bar{E}}_m(\epsilon,\sigma,\bar{x},t)\cdot\bar{E}_m(\epsilon,\sigma,\bar{x},t)dt, \tag{2.6}$$

where $\bar{E}_m(\epsilon,\sigma,\bar{x},t)$ is the numerically computed E-field in the area where equivalent dielectric properties are searched for and $\tilde{\bar{E}}_m(\epsilon,\sigma,\bar{x},t)$ is the solution to the adjoint problem with the residual between the computed field and $\bar{E}_m^{meas}(\bar{R}_n,t)$ as sources. $\langle\sigma\rangle$ is a parameter compensating for the different scaling of the gradients.

Since the phase of the measured field is unknown, we have here modified the algorithm slightly so that the phase of $\bar{E}_m^{meas}(\bar{R}_n,t)$ is set to be

equal to that of $\bar{E}_m(\epsilon, \sigma, \bar{R}_n, t)$ at each iteration step of the procedure. The amplitudes of $\bar{E}_m^{meas}(\bar{R}_n, t)$ are obtained from the measurements.

Results for the adjoint field method can be found in the papers **A** and **E**. Summaries of the two papers are given in 4.1 and 4.5.

2.2.2 The phase angle gradient method

The phase angle gradient method is based on the field equivalence principle. Detailed descriptions of this principle can be found in for example [18] and [50]. The field equivalence is, according to [18], a more rigorous formulation of Huygens' principle [51], that was introduced in 1936 by S. A. Schelkunoff [52].

According to the field equivalence principle there are some different equivalents that can be used to represent the actual electromagnetic source in figure 2.1. One option is to imagine that a surface S_c that encloses the source instead of its actual content is totally filled with a material that is a perfect electric conductor, see figure 2.3. If a magnetic current density $\bar{M}_{eq}$

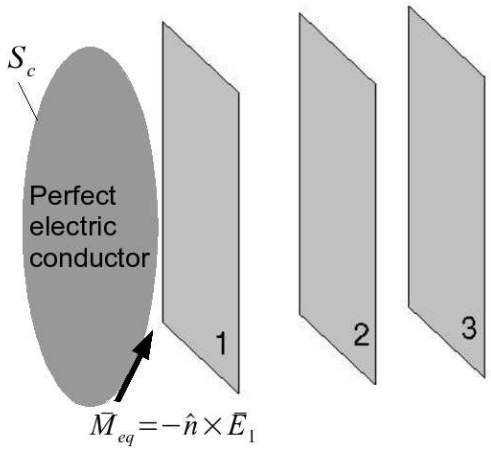

Figure 2.3: Equivalent that has the same fields outside the surface S_c as the original problem

then is placed on S_c and

$$\bar{M}_{eq} = -\hat{n} \times \bar{E}_1, \tag{2.7}$$

where $\hat{n}$ is a unit normal pointing out from S_c and $\bar{E}_1$ is the electric field that the actual source would give on S_c, the resulting field outside S_c would be the same as for the actual source.

The surface S_c can for example be chosen such that a part of S_c is a very large plane surface parallel to and close to plane 1. If plane 1 is chosen large enough, the field from the equivalent can be approximated with the field from a magnetic current density on plane 1 in front of an infinite perfectly conducting plane. By using mirroring the current density on plane 1 in front

of the perfectly conducting plane can be replaced by an equivalent magnetic surface current density on plane 1 in free space

$$\bar{M}_s = -2\hat{n} \times \bar{E}_{p1}, \tag{2.8}$$

where $\hat{n}$ is a unit vector perpendicular to plane 1 pointing towards the other planes and $\bar{E}_{p1}$ is the electric field on plane 1.

The electric vector potential from $\bar{M}_s$ in free space is

$$\bar{F} = \frac{\epsilon}{4\pi} \iint_S \bar{M}_s(\bar{r}')\, G(\bar{r}, \bar{r}')\, ds'. \tag{2.9}$$

Here, the surface S is plane 1, ϵ is the permittivity and $G(\bar{r}, \bar{r}')$ is the Green's function

$$G(\bar{r}, \bar{r}') = \frac{e^{-jk|\bar{r}-\bar{r}'|}}{|\bar{r}-\bar{r}'|}, \tag{2.10}$$

where k is the wavenumber. If the surface S is divided into a square grid with the grid cell area ΔS, the integral can be approximated as

$$\bar{F} \approx \frac{\epsilon}{4\pi} \sum_p \bar{M}_s(\bar{r}'_p)\, G(\bar{r}, \bar{r}'_p)\, \Delta S, \tag{2.11}$$

where $\bar{r}'_p$ represents the point in the middle of the grid cell number p. The electric field can then be calculated using equation (2.11) and the relation between $\bar{E}$ and $\bar{F}$. If the system of coordinates is chosen such that plane 1 is the xy-plane, the resulting expressions are

$$E_x = -\frac{\Delta S}{2\pi} \sum_p E_x(\bar{r}'_p) \frac{\partial G(\bar{r}, \bar{r}'_p)}{\partial z} \tag{2.12}$$

$$E_y = -\frac{\Delta S}{2\pi} \sum_p E_y(\bar{r}'_p) \frac{\partial G(\bar{r}, \bar{r}'_p)}{\partial z} \tag{2.13}$$

$$E_z = \frac{\Delta S}{2\pi} \sum_p \left(E_x(\bar{r}'_p) \frac{\partial G(\bar{r}, \bar{r}'_p)}{\partial x} + E_y(\bar{r}'_p) \frac{\partial G(\bar{r}, \bar{r}'_p)}{\partial y} \right). \tag{2.14}$$

If plane 1 is chosen large enough and ΔS small enough, the equations (2.12), (2.13) and (2.14) give good approximations for the fields on the planes 2 and 3.

The field amplitudes are known on plane 1, so the field on the other planes can be regarded as a function of the unknown phase angles of the tangential components of $\bar{E}$ on plane 1.

After the phase angles on plane 1 have been initiated, e.g. to be zero, the resulting field estimates on the planes 2 and 3 can be calculated. To find the correct phase, the initial angles are altered in small steps, so that the field amplitudes $|E_i|_n$, where n is a computational grid point, converge to the measured values $|E_i^m|_n$. A functional J of the phase can be defined as

$$J \equiv \frac{1}{2} \sum_n \left((|E_x|_n - |E_x^m|_n)^2 + \left(|E_y|_n - |E_y^m|_n\right)^2 + (|E_z|_n - |E_z^m|_n)^2 \right). \tag{2.15}$$

The phase angles are changed in the opposite direction of the phase angle gradients of J, so that J is minimized. To obtain expressions for the gradients, the analytical derivatives of J with respect to the phase angles in the measurement points on plane 1, are calculated. The phase angle gradient method is suitable for parallelization as many iterations are needed for convergence.

It can be noted that J, unlike the cost function in equation (2.3) for the method described in [23] and [24], contain all three field components and gives resulting phase angles from the minimization, that contain information on the phase difference between the different field components.

Although the phase angle gradient method originally was developed for calculation of the phase angles of the electric field from measured electric field amplitudes, it can, because of the symmetry of Maxwell's equations, also be used to calculate the phase angles of the magnetic flux density $\bar{B}$ from measured amplitudes of $\bar{B}$.

Results for the phase angle gradient method can be found in the papers **A** – **E**. Summaries of the papers are available in chapter 4.

2.3 Phase retrieval for field with low frequency

Phase retrieval is not only of interest for situations with high-frequency fields. It is also useful for modeling of sources with low-frequency electromagnetic fields, for which the distances between measurement planes become small in terms of wavelengths.

2.3.1 Earlier work

Earlier work with source modeling for low frequency applications have been performed by various authors. Source reconstruction for electromagnetic interference (EMI) studies, using both field amplitude and phase, is described in [53–55]. Attempts were made in [53] to do phase retrieval, but the results were not encouraging. The authors concluded that this was due to the long wavelengths of the radiated field. This problem is revisited in 2.3.2.

Baudry et al. [56] discussed near-field techniques in electromagnetic compatibility (EMC) investigations and presented results for a method in which equivalent electric dipoles are used for source modeling. It can also be mentioned that similar low-frequency inverse source problems are relevant for other fields of applications such as medical imaging by magnetoencephalography (MEG) [57] or magnetization identification [58].

2.3.2 The phase angle gradient method for low frequency

From the above discussion, it is clear that if phase retrieval can be performed even for situations with distances between the measurement planes that are small in terms of wavelengths, it is of large interest for EMC applications. Low-frequency phase retrieval is also interesting for electromagnetic dosimetry and it is demonstrated in the papers **B** and **C** that such phase retrieval really is possible with the phase angle gradient method (PAGM).

The PAGM works with distances between scanning surfaces much smaller than a wavelengths this is in apparent contradiction with results of [22]. It was reported in [22] that the distance between the scanning surfaces plays an important role in determining the lack or occurrence of local minima. Both theoretical investigations and experimental results were presented. A practical procedure for antenna testing was also described in which the distance between the scanning surfaces was chosen to be of the order of a few wavelengths. The method that was described in [22] is gradient based like the PAGM and a functional is minimized.

However, an important difference between the two methods is the choice of unknowns. In [22] the complex field was searched for and the functional is formulated so that the inverse problem becomes quadratic. In the PAGM we instead search for the correct phase angles that together with measured field amplitudes on one measurement plane, give correct calculated field amplitudes on two other planes. In other words, the unknowns that we are searching for in the PAGM are the phase angles, but not the complex fields. The tangential component of the electric field on the measurement plane closest to the source $\bar{E}_{tan}$ can be written as an expression containing the measured amplitudes and sinusoidal functions of the unknown phase. As discussed in section 2.2.2, the field on the other planes can be written in terms of $\bar{E}_{tan}$. This leads to an inverse problem with a nonlinearity that is not quadratic. So although the basic goal for the PAGM and the method in [22] are to find the correct field from amplitude measurements, they are quite different mathematically. Thus the results in [22] does not provide information about whether the PAGM works for cases with plane distances much smaller than the wavelength or not.

In this chapter we have described different phase retrieval methods. Next chapter contains a discussion of electromagnetic calculations.

Chapter 3

Electromagnetic calculations

Solving Maxwell's equations is required both in phase retrieval methods and in dosimetry calculations. Maxwell's equations can be written

$$\nabla \cdot (\mu \bar{H}) = 0 \tag{3.1}$$

$$\nabla \cdot (\epsilon \bar{E}) = \rho \tag{3.2}$$

$$\nabla \times \bar{H} = \bar{J} + \epsilon \frac{\partial \bar{E}}{\partial t} \tag{3.3}$$

$$\nabla \times \bar{E} = -\mu \frac{\partial \bar{H}}{\partial t}, \tag{3.4}$$

where $\bar{E}$ is the electric field intensity, $\bar{H}$ the magnetic field intensity, $\bar{J}$ the current density, ρ the volume charge density, ϵ the permittivity and μ the permeability.

There are several different numerical methods, that can be used to solve these equations. Some examples are the impedance method [16], the finite-difference time-domain (FDTD) method [15], the Finite Integration Theory [59], the Finite-Volume Time-Domain (FVTD) method [60], the HD-FDTD method [61], the finite-element method (FEM), the method of moments (MoM), the hybrid finite-element method (FEM)/method of moments (MoM) technique described in [17] and the FEM-FDTD hybrid method that can be found in [62].

In situations with exposure to low frequency fields, one suitable method is the impedance method described in [16, 63, 64]. For high frequency fields the finite-difference time-domain (FDTD) method [15] is very suitable. Another method that can be used is the finite-element method. In [17] is for example a hybrid finite-element method (FEM)/method of moments (MoM) technique employed for SAR calculations in a human phantom in the near field of a base-station antenna.

Once the electromagnetic fields inside the human have been calculated, SAR and induced current density can be calculated and comparisons can be made with the exposure safety guidelines.

3.1 The FDTD method

For high frequencies the finite-difference time-domain (FDTD) method is suitable. It was first presented by Yee in [15]. Further information about the method can be found in for example [65]. One suitable application for FDTD is for example mobile phone dosimetry. The use of FDTD for low frequencies is limited by the large number of time steps that then is required, if FDTD is used in the standard way. Methods have however been developed, that makes it possible to also use FDTD for low frequencies, see [61, 66].

The FDTD method deals with numerical approximations of Maxwell's equations in space and time using a staggered grid for the $\bar{E}$ and $\bar{H}$ components of the field. The computational space is divided in cells of the kind that are shown in figure 3.1. The positions where the field components are

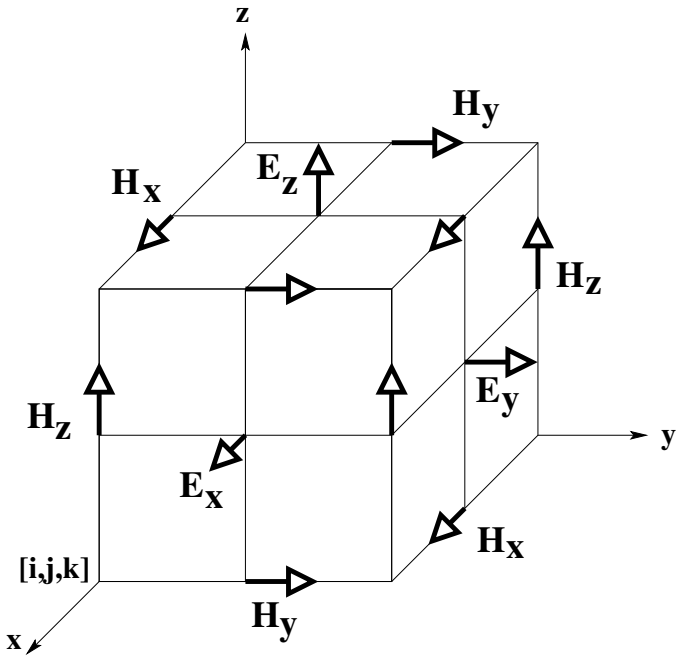

Figure 3.1: The Yee cell.

evaluated are indicated in the figure. In the standard Yee cell the $\bar{E}$ components are placed on the edges and the $\bar{H}$ components on the faces, the alternative Yee cell shown in figure 3.1 is suitable when subgridding is used for modeling of biological tissues [67].

The electric field vector components E_x, E_y and E_z and the magnetic field vector components H_x, H_y and H_z are located in the computational space so that each $\bar{H}$ component is surrounded by four circulating $\bar{E}$ components and each $\bar{E}$ component is surrounded by four circulating $\bar{H}$ components, see figure 3.1.

All the $\bar{E}$ components for a particular time are calculated using $\bar{H}$ from a

previous time point and the previous values of the $\bar{E}$ components. Then all of the $\bar{H}$ components are updated using the $\bar{E}$ field just computed. This cycle is then repeated during the simulation time. Equations for time stepping of the different field components can be derived using the integral forms of the equations (3.3) and (3.4).

To demonstrate how this can be done, it is here shown how the time stepping equation for the H_z component can be obtained. The integral form of equation (3.4) can be written

$$\oint_C \bar{E} \cdot d\bar{l} = -\mu \frac{\partial}{\partial t} \iint_S \bar{H} \cdot d\bar{S}. \tag{3.5}$$

This equation can be applied on the H_z component and the $\bar{E}$ components that surround it. If the $\bar{E}$ components are considered constant along the sides of a rectangular loop around H_z and H_z is considered constant on the area bounded by this loop, we can write

$$\begin{aligned} &-\left(E^{n+1/2}_{x[i,j+1/2,k+1/2]} - E^{n+1/2}_{x[i,j-1/2,k+1/2]}\right)\Delta x \\ &+\left(E^{n+1/2}_{y[i+1/2,j,k+1/2]} - E^{n+1/2}_{y[i-1/2,j,k+1/2]}\right)\Delta y = \\ &\qquad -\mu \frac{H^{n+1}_{z[i,j,k+1/2]} - H^{n}_{z[i,j,k+1/2]}}{\Delta t}\Delta x \Delta y. \end{aligned} \tag{3.6}$$

Here the indices $|_{i,j,k}$ refer to the x, y and z coordinates and $|^n$ refer to the time coordinate such that

$$U^n_{[i,j,k]} = U(i\Delta x, j\Delta y, k\Delta z, n\Delta t), \tag{3.7}$$

where $\Delta x \times \Delta y \times \Delta z$ is the size of the Yee cell, Δt is a time increment and U is a field component. The $\bar{H}$ components are evaluated for integer time indexes $1, 2, 3, \ldots$ and the $\bar{E}$ components for half-integer time indexes $1/2, 3/2, 5/2, \ldots$. From equation (3.6) an expression for $H^{n+1}_{z[i,j,k+1/2]}$ can easily be obtained.

It can be shown [68] that in order to ensure stability of the FDTD solution the time step Δt has to fulfill the condition

$$\Delta t \leq \frac{1}{c}\left(\frac{1}{\Delta x^2} + \frac{1}{\Delta y^2} + \frac{1}{\Delta z^2}\right)^{-\frac{1}{2}}, \tag{3.8}$$

where c is the maximum wave phase velocity expected within the model.

In many electromagnetic problems of interest the spatial domain of the computed field is unbounded in one or more coordinate directions, so different kinds of absorbing boundary conditions have been developed over the years. Highly absorbing boundary conditions have been presented by Mur [69].

Later Berenger presented a perfectly matched layer (PML) for absorption of electromagnetic waves [70]. In previous techniques a wave is absorbed

without reflection only in particular cases, for example, if it is plane and has a propagation direction that is perpendicular to the boundary [70]. For the PML medium suggested by Berenger, on the other hand, the theoretical reflection factor of a plane wave that hit a vacuum-layer interface is null at any incidence angle [70].

A more recent development is the CPML formulation presented in [71]. The CPML offers advantages over traditional PML implementations. It is highly absorptive of evanescent modes and it does not require modifications when applying it to inhomogeneous, lossy, anisotropic, dispersive or nonlinear media [71].

3.2 Insertion of source model

If the field from an electromagnetic source in free space is obtained using a suitable phase-retrieval method as described in chapter 2 and an appropriate method to compute the field in a human exposed to the source is chosen, the next step is to insert the obtained field in the computation in a suitable way.

An important issue to consider then is how much the field is perturbed by the presence of a human. If the measured field in front of the source is a magnetic field with low frequency, a reasonable approximation is, due to the nonmagnetic nature of the human body, to assume that the presence of the body does not perturb the magnetic field from the source significantly. For a field with high frequency on the other hand it can be necessary to take into account the presence of the human by using a total-field/scattered-field formulation [65, 69, 72]. This is effective provided that the distance between the human and the source is such that the source is insignificantly affected by the presence of the human.

This kind of formulation is often used, in other applications, in order to insert plane waves into FDTD computations. Figure 3.2 illustrates that the computational domain for an FDTD computation can be divided in two parts, the total field region and the scattered field region. The total field $\bar{E}^{tot}$ can be written

$$\bar{E}^{tot} = \bar{E}^{i} + \bar{E}^{s}, \tag{3.9}$$

where $\bar{E}^{i}$ is the incident field, that is the field that the source outside the computational domain would cause in free space, and $\bar{E}^{s}$ is the scattered field. The FDTD equations are used to update $\bar{E}^{tot}$ in the total field region and $\bar{E}^{s}$ in the scattered field region.

When the FDTD equations are evaluated for the total field at nodes inside, but adjacent to, the boundary for the total field region, the total field will be required from some nodes that are located outside this boundary. The equations for the relevant nodes are then modified so that when the total field inside the boundary is computed, the incident field is added to the scattered field that is obtained from nodes outside the boundary. Similarly,

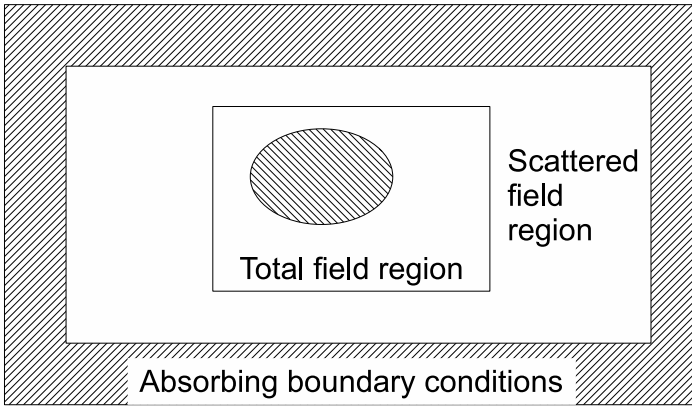

Figure 3.2: The computational domain can be divided in two parts, the total field region and the scattered field region.

when the scattered field is computed, the incident field is subtracted from the total field obtained from inside the total field region.

In summary a magnetic field with low frequency is not affected much by the presence of a human, whereas it should be taken into account that fields with high frequency can be affected by the presence of a human in front of the source.

Chapter 4

Summary of papers

In this chapter a brief summary of the papers included in the thesis is given.

4.1 Paper A

Two different methods to recreate the phase angles from measured field amplitudes on a set of parallel planes in the near field of an electromagnetic source, are presented in this paper. The first method, the adjoint field method, is a gradient-based optimization algorithm, based on the adjoint fields. The second method, the phase angle gradient method, employs an optimization algorithm based on the phase angle gradients of a functional.

Field values from an analytical formula for an infinitesimal dipole were used to evaluate the methods, instead of measurement data. A 2D test case, with the frequency 1 GHz, was used for the adjoint field method. The correct phase angles and the phase angles that the adjoint field method gives for the test case are shown in figure 4 in the paper. The phase angle gradient method was tested for 3D test cases with the frequencies 1 GHz and 100 MHz. The figures 6 and 7 in paper **A** show calculated and correct phase angles for the 1 GHz case. In the figures 8 and 9 differences between calculated and correct phase angles for the same case can be seen. The summed and weighted phase angle error, as defined by equation 14 in the paper, for the 1 GHz and 100 MHz test cases are shown as a function of iteration number in the figures 11 and 12. Note that there is a misprint in the caption of figure 11. It is written 16Hz, but it should be 1 GHz. It can be noted in the figures that much fever iterations were needed for the 100 MHz case, than for the 1 GHz case.

The phase angle gradient method and the adjoint field method worked well for the used test cases. The obtained summed and weighted phase angle error, as defined by equation 14 in the paper, for the phase angle gradient method is clearly below 0.1 rad. The methods are useful for modeling of electromagnetic sources and have the important advantage that they can be used for many different sources without detailed knowledge of the sources.

4.2 Paper B

This paper contains a performance evaluation of the phase angle gradient method that was presented in paper **A**. Phase retrieval based on field measurements for different plane sizes and separations between the planes are studied. Moreover the method is tested for different initial phase distributions. The results show that the phase retrieval works well, even if the separation between the measurement planes is small in terms of wavelengths.

Figure 3 in the paper shows results for a numerical test case with a source consisting of five infinitesimal dipoles. Retrieved and correct phase angles as well as the difference between them are shown. The results are for the measurement plane closest to the source, plane 1. It can be seen that the differences between calculated and correct phase angles are small, with the exception of some unimportant larger errors in areas near rapid changes in the phase and near the edges of the planes.

This is illustrated in figure 4, where correct field amplitudes and the difference between calculated and correct phase angles on plane 1 for E_x, one of the field components tangential to the measurement planes, are shown. Small errors in the calculated phase can be observed at places where the field amplitudes are large. Larger errors can be seen at places with smaller amplitudes where the value of the phase not are important. Figure 5 and 6 illustrate that the calculated phase that the retrieved phase on plane 1 gives on the next plane agrees well with the correct phase.

Figure 7 shows the summed and weighted phase angle errors, as defined in equation 10, and the cost functions as function of iteration number, for two different initial phase distributions. Both the phase distributions gave small errors.

The phase angle gradient method was also tested for some test cases with an infinitesimal dipole as source. To test the performance for the method an initial test case was used, then the dimensions for that case, see figure 1 in the paper, were increased with the same scale factor. That is the sides of the measurement planes, the distances between them as well as the distance to the source from the planes, were all scaled up by the same factor, while the same source as in the first test case was kept. Figure 8 shows summed and weighted phase angle errors for different scaling factors. The figure shows small errors for distances between plane 1 and plane 2 that are smaller than 0.5λ. Even for a separation between the planes as small as in the scale of $10^{-9}\lambda$ the error is small. For the distances 0.5λ and 0.7λ the errors are larger.

To investigate further what is happening for the case with the distance 0.5λ between the first two planes, different initial phase distributions were tested. One distribution with the initial value zero for all the phase angles and two distributions with random phase were used. Four phase distributions with random numbers in different intervals were also used. The resulting summed and weighted phase angle errors can be found in figure 9.

The figure illustrates that small errors can be obtained for some of the intervals that are small enough, but for the other initial values the errors become larger. To test whether the results could be improved, more iterations were run. Figure 10 shows how the summed and weighted phase angle error varies with the number of extra iterations, if the test case with initial phase angles zeros is continued with more iterations. The results for three different cases where the phase, before the extra iterations, in each point is set to a random number in an interval around the obtained phase for the first simulation part, are also shown in figure 10. The errors for the four cases decrease with the number of extra iterations, but the resulting errors are still clearly larger than the results, for cases with smaller distances between plane 1 and plane 2, in figure 8.

In summary the performance evaluation of the phase angle gradient method showed that the method is able to accurately retrieve the phase information for test cases with different sources as well as various separations between and sizes of the measurement planes. Moreover the method works well even if the separations between the planes are much less than a wavelength.

4.3 Paper C

In this paper the phase angle gradient method, that was presented in paper **A**, was tested for magnetic flux density $\bar{B}$ with the frequency 50 Hz. The method was tested with both field values calculated with an analytical formula and measured field in front of a transformer. A robot was utilized to move a measurement probe between the measurement points in front of the transformer, see figure 8 in the paper.

The field from a vertical infinitesimal dipole was used to test the phase retrieval. Phase angles obtained with the phase angle gradient method, correct phase angles and difference between retrieved and correct phase are shown in figure 2. It can be seen that there is a good agreement between the retrieved and the correct phase. To investigate whether the phase angle gradient method works well for different initial values for the phase angles, the test case was run for some different initial values. Figure 3 shows the functional J, as defined by equation 6 in the paper, as function of iteration number for seven different initial phase distributions. In figure 4 the obtained summed and weighted phase angle error, as defined by equation 7 in the paper, as function of iteration number for the different initial phase distributions are shown. It can be seen that the method works well for the different phase distributions. Figure 5 shows retrieved phase, correct phase and the difference between them for a test case with an off-centered infinitesimal dipole. It can be seen that the method performs well also for this case.

To test the phase angle gradient method with measured field, measure-

ment values from three vertical parallel planes in front of the transformer were used to calculate the phase angles, see figure 1 in the paper. Figure 9 shows the obtained phase angles for a case with 161 x 90 measurement points on plane 1 and 151 x 80 points on the other two planes. The distance between the points on each of the planes in vertical as well as in horizontal direction was 1 cm.

If the obtained phase angles are similar to the correct ones, they should give calculated field amplitudes that are similar to the correct ones. Therefore, the obtained phase angles on the plane closest to the transformer was used to calculate the field amplitudes on the other planes. To test the number of points needed to get a good result, the distance between the measurement points used in the phase-retrieval was varied, by omitting some of the measurement points. Figure 10 (a) in the paper shows ratios between the largest value of |calculated amplitude - measured amplitude| and the largest measured amplitude on plane 2 for B_x, B_y and B_z, as a function of distance between used measurement points. The corresponding ratios for plane 3 can be seen in figure 10 (b). It can be seen that the errors are small for the distances up to 7 cm, but that larger errors occur for the distance 10 cm.

For the distance of 2 cm between the used measurement points, field amplitudes on another plane further away from the source than plane 3 were also calculated. The measured field on this fourth plane were not used in the calculation of the phase. In the figures 13 – 15 measured field amplitudes and the differences between calculated and measured amplitudes are shown for the different field components on the fourth plane. It can be seen that the differences are small compared to the measured field amplitudes. The ratios between the largest amplitude difference and the largest measured amplitude, as defined in equation 9 in the paper, for B_x, B_y and B_z for the fourth plane are for example 6.62 %, 9.51 % and 6.40 % respectively.

The phase angle gradient method worked well both for the numerical test case and for the case with measured field values in front of a transformer. The results in this paper together with the previous results in paper **A** show that the phase angle gradient method is very versatile, since it can be used for both high and low frequencies.

4.4 Paper D

This paper contains results for the phase angle gradient method for a test case with a mobile phone. Field values measured with the dosimetric assessment system DASY4 on a set of planes above the phone were used to calculate the phase angles of the electric field, see figure 1 in paper **C**. The measured field values were obtained from Ericsson Research in Stockholm.

Measurement values from the three planes that are closest to the phone were used to calculate the phase angles. Only 6 x 11 measurement points

were used on each plane. Therefore the measured field was interpolated before the phase angle gradient method was used to calculate the phase. The obtained phase angles on the measurement plane that is closest to the phone were used to calculate the RMS values of the field on the two other planes that were used in the calculation of the phase, plane 2 and 3, and on another measurement plane that was not used in the calculations of the phase angles, plane 4. Interpolated measured RMS values and the differences between calculated RMS values and the interpolated measured values for E_y on plane 4 are shown in figure 2 of paper **C**. Figure 3 and 4 show the corresponding results for E_x on all the planes where the RMS values were calculated and for E_z on plane 4.

As illustrated by the figures, the phase angle gradient method worked well for the test case. The obtained phase gave calculated field values that are similar to the correct values for E_y and E_z on plane 4 and for E_x on the planes 2 and 3. Since quite few measurement points were used in the calculation of the phase angles, it is probably possible to improve the results for E_x on plane 4, if more measurement points and larger planes are used.

4.5 Paper E

The adjoint field method and the phase angle gradient method are compared in this paper. The two phase retrieval methods were previously presented in paper **A**, but only a 2D implementation of the adjoint field method was available. In this study a 3D version of the adjoint field method is presented and compared with the other method. The 3D implementation of the adjoint field method was tested both with a test case with chosen dielectric properties and with field from an infinitesimal dipole.

In the case with chosen dielectric properties the field amplitudes on plane 1, see figure 1 in the paper, for one Cartesian component tangential to the plane, E_y, was set to 1 V/m on the plane. The amplitudes of the other tangential field component, E_x, was set to zero on the plane. The phase for E_x and E_y was also set to zero on the plane. A dielectric box with $\epsilon_r = 2$ was inserted in the volume between plane 1 and 2. The chosen field on plane 1 was used as source with the frequency 250 MHz. FDTD was used to calculate the field that the source together with the chosen dielectric properties gave on the other planes. The field amplitudes of E_y on three planes were then used to try to retrieve the phase of the field and the dielectric properties between plane 1 and 2. In figure 3 the retrieved phase for E_y on plane 2 and the difference between the retrieved and the correct phase are shown. It can be seen that the error for the phase is small. Figure 2 shows cross sections of the retrieved ϵ_r and the correct ϵ_r. It can be noticed that the retrieved ϵ_r is somewhat lower than the correct ϵ_r, but the retrieved object is also larger than the correct object in z-direction. More sources and receivers placed on different sides of the dielectric box could

probably improve the reconstruction of ϵ_r.

The adjoint field method was also tested with 500 MHz field from an infinitesimal dipole. Figure 4 (a) shows correct phase angles calculated with an analytical formula. In figure 4 (b) the phase that was retrieved with the adjoint field method is shown. The phase angle gradient method was also tested with field from the infinitesimal dipole. The resulting retrieved phase and the difference between the retrieved and the correct phase are shown in figure 4 (c) and (d). It can be seen in figure 4 that the phase angle gradient method performed better than the adjoint field method. Moreover it gave results that are in excellent agreement with the correct phase.

Chapter 5

Conclusions

Two methods to recreate the phase angles from measured field amplitudes, the adjoint field method and the phase angle gradient method, have been presented in paper **A**. The methods were tested with good results for test cases with field values from an analytical formula. A performance evaluation of the phase angle gradient method has been described in **B**. The method worked well for different sources as well as for different sizes of and distances between the measurement planes. The results showed that the method is capable of retrieving phase information even if the separations between the planes are small in terms of wavelengths. The phase angle gradient method was also tested for measured magnetic flux density with low frequency from a transformer, in paper **C**, and for electric field with high frequency from a mobile phone, in paper **D**. For the cases with measured field the obtained phase angles on the measurement plane closest to the source gave calculated fields on other measurement planes that agree well with measured fields. The comparison in paper **E** showed that the phase angle gradient method gave much better result than the adjoint field method.

The developed methods are very useful in situations with an electromagnetic source that is too hard or time consuming to make an accurate model of. Applications where phase retrieval is useful include electromagnetic dosimetry, electromagnetic compatibility investigations, near-field to far-field transformations and antenna diagnostics. In view of the many kinds of electromagnetic sources that are present in the world around us, an important advantage with the methods is that they can be used for many different sources without detailed knowledge of the sources.

A limitation with the phase angle gradient method is that in some exposure situations the distance between the human and the source can be such that the source is significantly affected by the presence of the human and then it may not work so well to insert the obtained free space field with the total-field/scattered-field formulation. Therefore, it would be interesting to investigate if the phase angle gradient method can be extended, to take into account the presence of the human in the calculations of the phase angles.

It could also be of interest to compare required number of measurement points for phaseless source modeling with the needed number of points if both amplitude and phase are measured, in different situations. The best choice may sometimes be to measure only amplitudes to avoid complicated and expensive phase measurements, whereas it possibly sometimes could be worth to measure the phase in order to decrease the required number of measurement points.

Possible future work include to use retrieved phase angles in different applications, for example in calculations of SAR and current density in humans exposed to different electromagnetic sources.

References

[1] A. Ahlbom, A. Green, L. Kheifets, D. Savitz and A. Swerdlow, "Epidemiology of Health Effects of Radiofrequency Exposure", *Environmental Health Perspectives*, vol. 112, no. 17, pp. 1741–1754, 2004.

[2] M. Feychting, A. Ahlbom and L. Kheifets, "EMF and health", *Annual Review of Public Health*, vol. 26, pp. 165–189, 2005.

[3] IARC Monographs on the Evaluation of Carcinogenic Risks to Humans, Non-Ionizing Radiation, Part 1: Static and Extremely Low-Frequency (ELF) Electric and Magnetic Fields, vol. 80, IARCPress, Lyon, France, 2002

[4] WHO: Extremely Low Frequency Fields Environmental Health Criteria Monograph No.238, 2007.

[5] Exposure to high frequency electromagnetic fields, biological effects and health consequences (100 kHz-300 GHz) - Review of the Scientific Evidence and Health Consequences. Munich: International Commission on Non-Ionizing Radiation Protection; 2009. ISBN 978-3-934994-10-2. http://www.icnirp.de/PubEMF.htm

[6] The INTERPHONE Study Group, "Brain tumour risk in relation to mobile telephone use: results of the INTERPHONE international case-control study", *International Journal of Epidemiology*, Vol. 39, no. 3, pp. 675-694, 2010.

[7] M. J. Schoemaker, A. J. Swerdlow, A. Ahlbom, A. Auvinen, K. G. Blaasaas, E. Cardis, H. C. Christensen, M. Feychting, S. J. Hepworth, C. Johansen, L. Klaeboe, S. Lönn, P. A. McKinney, K. Muir, J. Raitanen, T. Salminen, J. Thomsen and T. Tynes, "Mobile phone use and risk of acoustic neuroma: results of the Interphone case-control study in five North European countries", *British journal of cancer*, vol. 93, no. 7, 2005.

[8] International Commission on Non-Ionizing Radiation Protection, "Guidelines for limiting exposure to time-varying electric, magnetic, and electromagnetic fields (up to 300 GHz)", *Health Phys.*, vol. 74, no. 4, pp. 494–522, 1998.

[9] P. Dimbylow and W. Bolch, "Whole-body-averaged SAR from 50 MHz to 4 GHz in the University of Florida child voxel phantoms", *Physics in Medicine and Biology*, vol. 52, no. 22, pp. 6639–6649, 2007.

[10] Europa, Summaries of EU legislation, Exposure to electromagnetic fields, http://europa.eu/legislation_summaries/employment_and_social_policy/health_hygiene_safety_at_work/c11150_en.htm

[11] Commission to postpone and amend electromagnetic fields legislation to protect MRI, http://europa.eu/rapid/pressReleasesAction.do?reference=IP/07/1610&

[12] EUR-Lex, Directive 2008/46/EC, http://eur-lex.europa.eu/LexUriServ/LexUriServ.do?uri=OJ:L:2008:114:0088:01:EN:HTML

[13] IEEE Standard for Safety Levels with Respect to Human Exposure to Radio Frequency Electromagnetic Fields, 3 kHz to 300 GHz, Copyright 2006 by the Institute of Electrical and Electronics Engineers, Inc., New York, USA.

[14] Evaluating Compliance with FCC Guidelines for Human Exposure to Radiofrequency Electromagnetic Fields, OET Bulletin 65, Edition 97-01, Federal Communications Commission Office of Engineering & Technology, http://www.fcc.gov/Bureaus/Engineering_Technology/Documents/bulletins/oet65/oet65.pdf

[15] K. S. Yee, "Numerical Solution of Initial Boundary Value Problems Involving Maxwell's Equations in Isotropic Media", *IEEE Trans. Antennas and Propagation*, vol. 14, no. 3, pp. 302–307, 1966.

[16] J. F. Deford and O. P. Gandhi, "An Impedance Method to Calculate Currents Induced in Biological Bodies Exposed to Quasi-Static Electromagnetic Fields", *IEEE Trans. Electromagnetic Compatibility*, vol. 27, no. 3, pp. 168–173, 1985.

[17] F. J. C. Meyer, D. B. Davidson, U. Jakobus and M. A. Stuchly, "Human Exposure Assessment in the Near Field of GSM Base-Station Antennas Using a Hybrid Finite Element/Method of Moments Technique", *IEEE Transactions on Biomedical Engineering*, vol. 50, no. 2, pp. 224–233, 2003.

[18] C. A. Balanis, *Antenna Theory Analysis and Design*, John Wiley & Sons, Inc., New York, 1997.

[19] NARDA STS: Home, http://www.narda-sts.de/index.php

[20] EnviroMentor – EnviroMentor English, http://www.enviromentor.se/page24564.html

[21] T. Isernia, G. Leone and R. Pierri, "Results for a truncated phaseless near field technique", *Electronics Letters*, vol. 29, no. 5, pp. 505–506, 1993.

[22] T. Isernia, G. Leone and R. Pierri, "Radiation Pattern Evaluation from Near-Field Intensities on Planes", *IEEE Transactions on Antennas and Propagation*, vol. 44, no. 5, pp. 701–710, 1996.

[23] T. K. Sarkar and F. Las-Heras, "A Direct Optimization Approach For Source Reconstruction NF-FF Using Amplitude Only Data", *IEEE International Symposium on Electromagnetic Compatibility*, vol. 1, pp. 399–402, 2001.

[24] F. Las-Heras and T. K. Sarkar, "A Direct Optimization Approach for Source Reconstruction and NF-FF Transformation Using Amplitude-Only Data", *IEEE Transactions on Antennas and Propagation*, vol. 50, no. 4, pp. 500–510, 2002.

[25] F. Soldovieri, A. Liseno, G. D'Elia and R. Pierri, "Global Convergence of Phase Retrieval by Quadratic Approach", *IEEE Transactions on Antennas and Propagation*, vol. 53, no. 10, pp. 3135–3141, 2005.

[26] R. W. Gerchberg and W. O. Saxton, "A Practical Algorithm for the Determination of Phase from Image and Diffraction Plane Pictures", *Optik*, vol. 35, no. 2, pp. 237–246, 1972.

[27] A. Tennant, G. Junkin and A. P. Anderson, "Antenna far-field predictions from two phaseless cylindrical near-field measurements", *Electronics Letters*, vol. 28, no. 23, pp. 2120–2122, 1992.

[28] R. G. Yaccarino and Y. Rahmat-Samii, "Phaseless Bi-Polar Planar Near-Field Measurements and Diagnostics of Array Antennas", *IEEE Transactions on Antennas and Propagation*, vol. 47, no. 3, pp. 574–583, 1999.

[29] J. Fridén, M. Siegbahn, B. Thors and L. Hamberg, "Quick SAR assessment using dual-plane amplitude-only measurement", *Proc. 'EuCAP 2006'*, Nice, France, 2006.

[30] S. Farhad Razavi and Y. Rahmat-Samii, "A New Look at Phaseless Planar Near-Field Measurements: Limitations, Simulations, Measurements, and a Hybrid Solution", *IEEE Antennas and Propagation Magazine*, vol. 49, no. 2, pp. 170–178, 2007.

[31] J. Fridén and H. Isaksson, "Robust phase-retrieval for quick SAR assessment using dual plane amplitude-only data", *EMB 07 Computational Electromagnetics Methods and Applications Conference proceedings*, Lund, Sweden, 2007.

[32] J. R. Fienup, "Phase retrieval algorithms: a comparison", *Applied Optics*, vol. 21, no. 15, pp. 2758–2769, 1982.

[33] A. Roczniak, E. M. Petriu and G. I. Costache, "3-D Electromagnetic Field Modeling Based On Near Field Measurements", *Quality Measurements: The Indispensable Bridge between Theory and Reality (No Measurements? No Science!) Joint Conference - 1996: IEEE Instrumentation and Measurement Technology Conference and IMEKO Technical Committee 7. Conference Proceedings (Cat. No.96CH35936)*, vol. 2, pp. 1124–1127, 1996.

[34] A. Taaghol and T. K. Sarkar,"Near-field to near/far-field transformation for arbitrary near-field geometry, utilizing an equivalent magnetic current", *IEEE Transactions on Electromagnetic Compatibility*, vol. 38, no. 3, pp. 536–542, 1996.

[35] F. Las-Heras, M. R. Pino, S. Loredo, Y. Alvarez and T. K. Sarkar, "Evaluating near-field radiation patterns of commercial antennas", *IEEE Transactions on Antennas and Propagation*, vol. 54, no. 8, pp. 2198–2207, 2006.

[36] S. Blanch, L. Jofre and J. Romeu, "Comparation between classical and equivalent current approach near-field to far-field transformation", *IEEE Antennas and Propagation Society International Symposium. 1995 Digest (Cat. No.95CH35814)*, vol. 1, pp. 260–263, 1995.

[37] J. Romeu, L. Jofre, M. Ferrando, M. Baquero and J. Clavera, "Linear array diagnostic from near-field measurements", *AP-S International Symposium 1989. 1989 International Symposium Digest: Antennas and Propagation (Cat. No.CH2654-2/89)*, vol. 1, pp. 68–71, 1989.

[38] J. Romeu, S. Blanch and L. Jofre, "Planar array diagnostic from cylindrical near-field measurements", *1990 International Symposium Digest. Antennas and Propagation. Institute of Electrical and Electronics Engineers. Merging Technologies for the 90's (Cat. No. 90CH2776-3)*, vol. 3, pp. 1318–1321, 1990.

[39] M. Serhir, P. Besnier and M. Drissi, "Antenna Modeling Based on a Multiple Spherical Wave Expansion Method: Application to an Antenna Array", *IEEE Transactions on Antennas and Propagation*, vol. 58, no. 1, pp. 51–58, 2010.

[40] M. Serhir, P. Besnier and M. Drissi, "An Accurate Equivalent Behavioral Model of Antenna Radiation Using a Mode-Matching Technique Based on Spherical Near Field Measurements", *IEEE Transactions on Antennas and Propagation*, vol. 56, no. 1, pp. 48–57, 2008.

[41] K. Persson, M. Gustafsson and G. Kristensson, "Reconstruction and visualization of equivalent currents on a radome using an integral representation formulation", *Progress In Electromagnetics Research B*, vol. 20, pp. 65–90, 2010.

[42] J. L. A. Quijano and G. Vecchi, "Improved-Accuracy Source Reconstruction on Arbitrary 3-D Surfaces", *IEEE Antennas and Wireless Propagation Letters*, vol. 8, pp. 1046–1049, 2009.

[43] J. L. A. Quijano and G. Vecchi, "Near- and Very Near-Field Accuracy in 3-D Source Reconstruction", *IEEE Antennas and Wireless Propagation Letters*, vol. 9, pp. 634–637, 2010.

[44] O. P. Gandhi and M. S. Lam, "An on-site dosimetry system for safety assessment of wireless base stations using spatial harmonic components", *IEEE Trans. Antennas and Propagation*, vol. 51, no. 4, pp. 840–847, 2003.

[45] T. Takenaka, T. Tanaka, H. Harada and S. He, "FDTD approach to time-domain inverse scattering problem for stratified lossy media", *Microwave and Optical Technology Letters*, vol. 16, no. 5, pp. 292–296, 1997.

[46] M. Gustafsson and S. He, "An optimization approach to two-dimensional time domain electromagnetic inverse problems", *Radio Sci.*, vol. 35, no. 2, pp. 525–536, 2000.

[47] A. Fhager and M. Persson, "Comparison of two image reconstruction algorithms for microwave tomography", *Radio Sci.*, vol. 40, Art.No. RS3017, 2005.

[48] A. Fhager, *Microwave Tomography*, Doctoral Thesis, Chalmers University of Technology, Göteborg, 2006.

[49] A. Fhager, S. K. Padhi and J. Howard, "3D Image Reconstruction in Microwave Tomography Using an Efficient FDTD Model", *IEEE Antennas and Wireless Propagation Letters*, vol. 8, pp. 1353–1356, 2009.

[50] C. A. Balanis, *Advanced Engineering Electromagnetics*, John Wiley & Sons, 1989.

[51] C. Huygens, *Traite de la Lumiere*, Leyeden, 1690. Translated into English by S. P. Thompson, London, 1912, reprinted by The University of Chicago Press.

[52] S. A. Schelkunoff, "Some Equivalence Theorems of Electromagnetics and Their Application to Radiation Problems", *Bell System Tech. J.*, vol. 15, pp. 92–112, 1936.

[53] M. Rodríguez, M. Hernando, Y. Álvarez, F. Las-Heras, L. F. Herrán and J. López, "Evaluation of the Sources Reconstruction Technique Applied to Magnetic Field Measurement in Power Electronic Circuits", *Power Electronics Specialists Conference, 2008. PESC 2008. IEEE*, pp. 529–534, 2008.

[54] M. M. Hernando, A. Fernández, M. Arias, M. Rodríguez, Y. Álvarez and F. Las-Heras, "EMI Radiated Noise Measurement System Using the Source Reconstruction Technique", *IEEE Transactions on Industrial Electronics*, vol. 55, no. 9, pp. 3258–3265, 2008.

[55] M. Rodríguez, M. M. Hernando, M. Arias, Y. Álvarez and F. Las-Heras, "Application of source reconstruction techniques and NF-FF transformations to estimate the EMI regulation compliance of a power electronic circuit", *Applied Power Electronics Conference and Exposition, 2008. APEC 2008. Twenty-Third Annual IEEE*, pp. 1741–1746, 2008.

[56] D. Baudry, C. Arcambal, A. Louis, B. Mazari and P. Eudeline, "Applications of the Near-Field Techniques in EMC Investigations", *IEEE Transactions on Electromagnetic Compatibility*, vol. 49, no. 3, pp. 485–493, 2007.

[57] S. Baillet, J. C. Mosher and R. M. Leahy, "Electromagnetic Brain Mapping", *IEEE Signal Processing Magazine*, vol. 18, no. 6, pp. 14–30, 2001.

[58] O. Chadebec, J. -L. Coulomb, G. Cauffet, J. -P. Bongiraud and S. Guerin, "Magnetization identification problem Illustration of an effective approach", *COMPEL: The International Journal for Computation and Mathematics in Electrical and Electronic Engineering*, vol. 23, no. 2, pp. 518–530, 2004.

[59] T. Weiland, "Time Domain Electromagnetic Field Computation with Finite Difference Methods", *International Journal of Numerical Modelling: Electronic Networks, Devices and Fields*, vol. 9, pp. 295–319, 1996.

[60] K. S. Yee and J. S. Chen, "The Finite-Difference Time-Domain (FDTD) and the Finite-Volume Time-Domain (FVTD) Methods in Solving Maxwell's Equations", *IEEE Transactions on Antennas and Propagation*, vol. 45, no. 3, pp. 354–363, 1997.

[61] H. Zhao, S. Crozier and F. Liu, "A high definition, finite difference time domain method", *Applied Mathematical Modelling*, vol. 27, no. 5, pp. 409–419, 2003.

[62] T. Rylander and A. Bondeson, "Stability of Explicit-Implicit Hybrid Time-Stepping Schemes for Maxwell's Equations", *Journal of Computational Physics*, vol. 179, no. 2, pp. 426–438, 2002.

[63] N. Orcutt and O. P. Gandhi, "A 3-D Impedance Method to Calculate Power Deposition in Biological Bodies Subjected to Time Varying Magnetic Fields", *IEEE Transactions on Biomedical Engineering*, vol. 35, no. 8, pp. 577–583, 1988.

[64] O. P. Gandhi, "Some numerical methods for dosimetry: Extremely low frequencies to microwave frequencies", *Radio Science*, vol. 30, no. 1, pp. 161–177, 1995.

[65] A. Taflove and S. C. Hagness, *Computational Electrodynamics: The Finite-Difference Time-Domain Method*, Artech House, Boston, London, 2000.

[66] C. M. Furse and O. P. Gandhi, "Calculation of Electric Fields and Currents Induced in a Millimeter-Resolution Human Model at 60 Hz Using the FDTD Method", *Bioelectromagnetics*, vol. 19, no. 5, pp. 293–299, 1998.

[67] R. Kopecký, *Dosimetry of Local Radio Frequency Exposure*, Doctoral Thesis, Chalmers University of Technology, Göteborg, 2006.

[68] A. Taflove and M. E. Brodwin, "Numerical Solution of Steady-State Electromagnetic Scattering Problems Using the Time-Dependent Maxwell's Equations", *IEEE Transactions on Microwave Theory and Techniques*, vol. MTT-23, no. 8, pp. 623–630, 1975.

[69] G. Mur, "Absorbing Boundary Conditions for the Finite-Difference Approximation of the Time-Domain Electromagnetic-Field Equations", *IEEE Transactions on Electromagnetic Compatibility*, vol. EMC-23, no. 4, pp. 377–382, 1981.

[70] J.-P. Berenger, "A Perfectly Matched Layer for the Absorption of Electromagnetic Waves", *Journal of Computational Physics*, vol. 114, pp. 185–200, 1994.

[71] J. A. Roden and S. D. Gedney, "Convolution PML (CPML): An efficient FDTD implementation of the CFS-PML for arbitrary media", *Microwave and Optical Technology Letters*, vol. 27, no. 5, pp. 334–339, 2000.

[72] K. Umashankar and A. Taflove, "A Novel Method to Analyze Electromagnetic Scattering of Complex Objects", *IEEE Transactions on Electromagnetic Compatibility*, vol. EMC-24, no. 4, pp. 397–405, 1982.

Papers A–E